Extended Magnetohydrodynamic Simulations of Edge Localized Modes in Existing and Future Tokamak Devices

C.R. Sovinec 1) A.Y. Pankin 2) S.E. Kruger 3), D.P. Brennan 4), P.B. Snyder 5)
D.D. Schnack 1), E.D. Held 6), D.C. Barnes 7) G. Bateman 2), A.H. Kritz 2)
S.C. Jardin 9), J. Breslau 9)

1) University of Wisconsin-Madison, Madison, Wisconsin, USA
2) Lehigh University, Bethlehem, Pennsylvania, USA
3) Tech-X Corporation, Boulder, Colorado, USA
4) Tulsa University, Tulsa, Oklahoma, USA
5) General Atomics, San Diego, California, USA
6) Utah State University, Logan, Utah, USA
7) Los Alamos National Laboratory, Los Alamos, New Mexico, USA
8) University of Colorado, Boulder, Colorado, USA
9) PPPL, Princeton, New Jersey, USA

e-mail contact of main author: sovinec@engr.wisc.edu

Abstract.
Linear and nonlinear computations of peeling-ballooning modes are presented here using equilibria for the DIII-D and ITER tokamaks. Eigenvalue computations for the two configurations show similar stability properties, and a practical model for particle and energy loss is proposed. Numerical convergence is shown for time-dependent computations. Two-fluid results show stabilization at large toroidal wavenumber, consistent with analytical theory that considers the localized nature of the diamagnetic drift velocity. Initial nonlinear two-fluid results show evolution toward a helically localized structure, unlike previous single-fluid results.

1. Introduction

High-performance tokamak plasmas operate in the H-mode regime that is characterized by large edge plasma gradients. While the existence of the edge transport barrier that gives rise to these gradients improves the overall plasma confinement, the resultant free energy from the large gradients causes plasma instabilities, known as Edge Localized Modes (ELMs). Present planning may put ITER operation in the Type-I ELM regime, where power loads caused by the ELMs can limit the plasma divertor lifetime [1]. An important problem facing the fusion community is the optimization of ELMy H-mode operation while minimizing the deleterious effects of ELMs.

Theoretical progress in understanding ELMs has been made by investigating the stability boundaries of peeling-ballooning modes using an ideal MHD model [2, 3, 4, 5]. In this study, ideal-MHD peeling-ballooning stability analysis is carried out for a series of equilibria that are generated with the TEQ and TOQ equilibrium codes. The H-mode pedestal pressure and parallel component of plasma current density are varied in a systematic way in order to cover the relevant parameter space for a specific ITER discharge. The ideal MHD stability codes DCON, ELITE, and BALOO are employed to verify whether each equilibrium profile is unstable to either peeling or ballooning behavior in the pedestal region.

Linear ideal MHD calculations measure the sources of free energy, but more comprehensive models and nonlinear effects are needed to understand ELM events. Time-dependent computations with the extended-MHD code NIMROD [6] allow us to consider two-fluid effects and nonlinear mode coupling. Though solved in single-fluid form [7], Hall and ∇p_e terms may be included in the electric field, and flow velocity evolution may include Braginskii gyroviscous stress. Anisotropic thermal conduction may be used in either two-fluid or resistive MHD computations with NIMROD.

2. Linear Studies and Numerical Convergence

Ideal ballooning codes have long been described in terms of an s-α diagram [8], which plots

a normalized pressure profile, α, against the normalized magnetic shear, *s*. With peeling-ballooning modes, the most unstable mode can occur at finite-n [2]. Here, it is more useful analyze stability with respect to parallel current density, $j_{||}$, because it more directly accesses the free energy available to drive the instabilities. To map out the instability diagrams for the H-mode plasma, the codes DCON [9], ELITE [2, 3], and BALOO [10] are used. DCON is used for the low n-modes (n<8), while ELITE is used for intermediate mode numbers, and BALOO is used for the infinite-n ballooning mode limit. In Fig. 1, the results of such a study are shown for a high triangularity DIII-D discharge and for an ITER discharge. While the geometry and plasma parameters for the ITER and DIII-D tokamaks are very different, the stability thresholds for these two tokamaks are surprisingly close to each other. There are still important differences between two stability diagrams in Fig. 1, such as wider second stability ballooning stability region for ITER, but the critical values for the normalized pressure gradient and the parallel component of current density are about the same. The peeling-ballooning stability results may be combined with a model for particle and heat losses during an ELM crash and a model for ELM width to provide a practical approach for integrated predictive modeling of ELMy H-mode plasmas [11]. Given the excellent diagnostic capabilities of the DIII-D tokamak, the following focuses on DIII-D, where experimental validation is possible and necessary before extrapolating to ITER parameters.

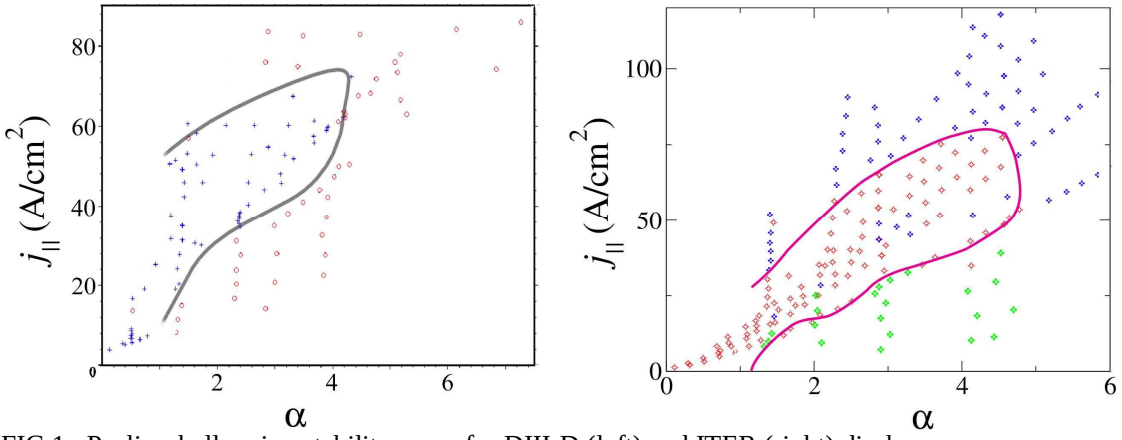

FIG 1. Peeling-ballooning stability maps for DIII-D (left) and ITER (right) discharges.

With their broad range of unstable toroidal mode numbers of order 10 and radial localization to where the q-value increases sharply, ELMs tend to have high poloidal mode numbers (m). The radial localization coincides with the large pressure and current density gradients that drive the modes. In this work, we use MHD equilibria fitted to experimental data from the DIII-D discharge 113317. The flux surface profiles are shown in Fig. 2, including the density profiles that is based on laboratory measurements. Both the temperature profile and the number density profile drop by approximately a factor of four from just inside to outside the separatrix. To satisfy MHD equilibrium in the edge plasma region beyond the separatrix, the temperature and number density are considered uniform at the values provided by the equilibrium file for the separatrix (T_e = 100 eV and n = 1.2x10^{19} m^{-3}, respectively).

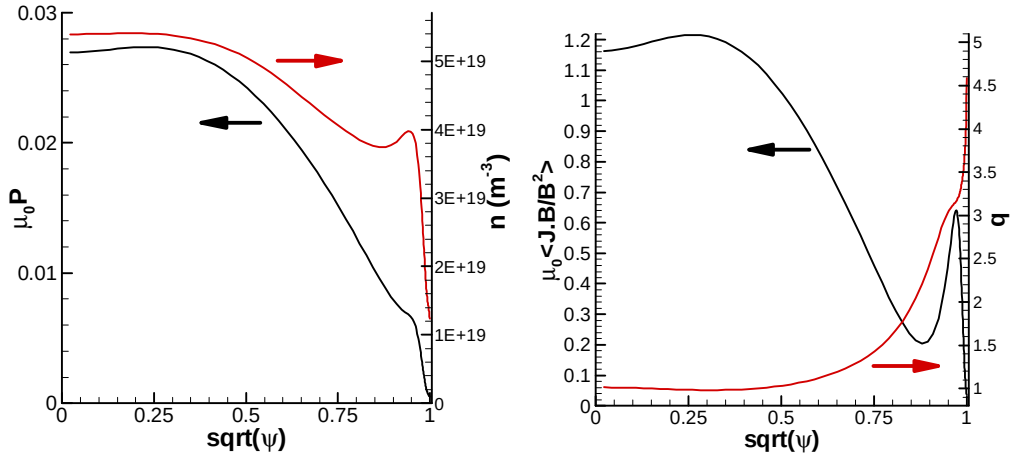

FIG 2. Flux-surface profiles for the equilibrium fit to the DIII-D discharge 113317. Equilibrium pressure and number density are shown on the left, and average parallel current density and safety factor are shown on the right.

Before discussing linear results, we consider numerical convergence properties for the NIMROD algorithm on the radially localized, high-poloidal-wavenumber ELMs. The code uses high-order quadrilateral finite elements for the poloidal plane, and finite Fourier series for the toroidal direction. The finite element grid is non-uniform, and we find it advantageous to pack the elements radially near the separatrix, leaving the core with relatively large elements. The mesh is well-aligned with the equilibrium magnetic flux except near the separatrix and in the open-field region. The boundary of the domain conforms to the shape of the closed flux surfaces and is located at approximately the same average distance from the separatrix as the wall in the experiment. Convergence with respect to spatial resolution has been confirmed by changing the number of elements in the mesh and by varying the order of the polynomial basis functions from two (biquadratic elements) to eight. The numerical representation of vector fields does not identically satisfy the divergence constraint for the magnetic field, and numerical diffusion is used to control errors [6]. Thus, we check for decreasing magnetic divergence error, in addition to convergence on a mode's growth rate, when testing resolution.

Results for three representative wavenumbers, computed with the resistive MHD model and anisotropic heat conduction, are shown in Fig. 3. The resistivity profile is based on the Spitzer model applied to the equilibrium temperature but multiplied by a constant to make $\eta/\mu_0 \cong 7.0$ m^2/s in the pedestal region. The anisotropic heat conduction has $\chi_{\|}$=1.5×10^7 m^2/s and $\chi_{\perp}$=1.5 m^2/s, and there is an artificial particle diffusivity of D_n = 2.5 m^2/s. Figure 3 shows that high-order polynomials are needed to achieve convergence with the 20×128 mesh. The modes with the largest n-values require the greatest poloidal resolution to achieve convergence, as expected from the resonance condition of $m=qn$. The finer poloidal structure of the n=42 mode relative to the n=21 mode is evident from the computed eigenfunctions (Fig. 4). The larger n-value modes also have larger growth rates, a ballooning-like character that is not in agreement with ideal-MHD results for the same equilibrium. This may result from finite resistivity, which is included in the NIMROD computations; further study is warranted.

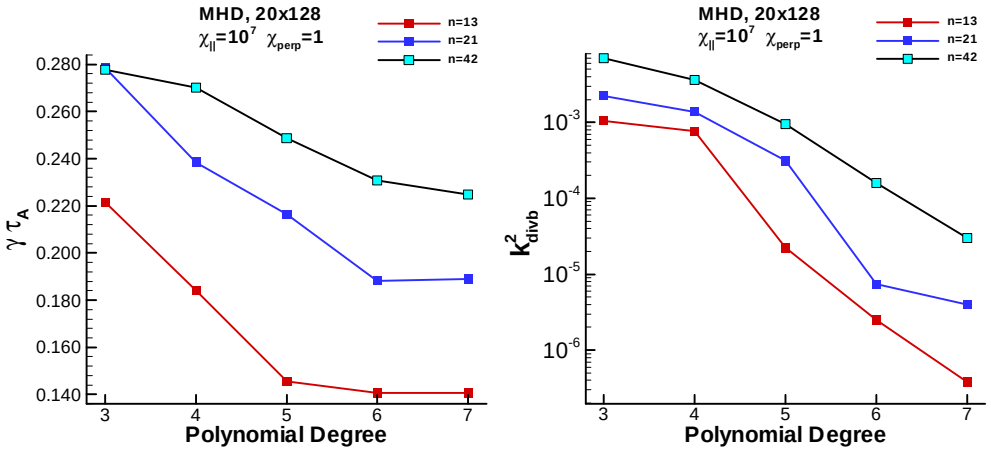

FIG 3. Computed growth-rate and divergence error, measured as $\int(\nabla\cdot\tilde{b})^2\,dVol\,/\int\tilde{b}^2\,dVol$, for three modes in the resistive MHD spectrum with anisotropic thermal conduction (values are divided by 1.5). The pedestal electrical diffusivity is 7 m^2/s, ν=25 m^2/s, Δt=5×10^{-8} s, and D=2.5 m^2/s.

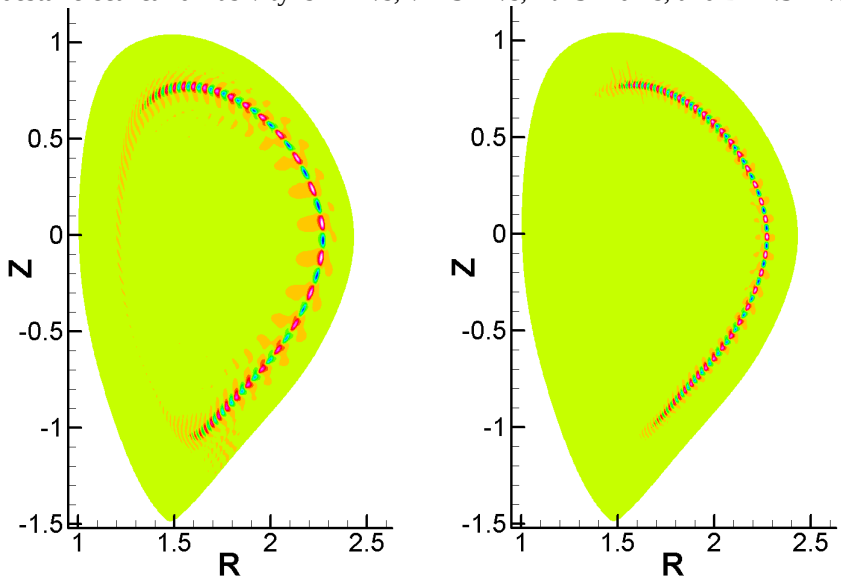

FIG 4. Toroidal component of flow velocity from the resistive MHD eigenmodes of the n=21 mode (left) and n=42 mode (right), computed with polynomial basis functions of degree 6.

Resolution requirements with the two-fluid electric field and gyroviscosity are more stringent, but the stabilizing effect of diamagnetic rotation leads to a growth-rate spectrum that peaks at moderate n-value. Convergence studies similar to those shown in Figs. 3 have been performed for this model. At the parameters used for MHD, the peak of the two-fluid spectrum also converges. Increasing the particle diffusivity to 5 m^2/s facilitates convergence for the largest n-values, and we find that modes with n≥30 are not growing modes. The most unstable modes have toroidal wavenumbers between 10 and 20, as shown in Fig. 5, the computed growth-rate spectrum for n≤42. Resistive MHD results for the same parameters are also shown. Estimating the point of two-fluid stabilization from slab geometry analysis [12] does not explain the two-fluid threshold. The poloidal component of diamagnetic drift velocity ($\mathbf{B}\times\nabla p/neB^2$, plotted in Fig. 6) peaks at nearly 4×10^4 m/s. With the analytical estimate from Ref. 12 suggesting stability at $\omega_{*i}=\mathrm{m}v/r=2\gamma_{MHD}$, the observed MHD growth-rate of approximately 2×10^5 s^{-1}, minor radius $r\cong 0.5$ m, and q-value of approximately 3, one might

expect stability at n=m/*q* of order unity. However, the radial extent of the diamagnetic drift is narrower than the ELM eigenfunctions, and radial localization is known to reduce the stabilizing effect of ion diamagnetic drift [13]. For the modes remaining unstable, two-fluid effects lead to visible distortion of the eigenfunctions. The flow pattern of the n=21 mode, for example, is significantly sheared along the outboard portion of its resonant surface (Fig. 6; compare with the n=21 mode shown in Fig. 4), which is the location of peak diamagnetic drift. The growth rate of this mode is 5% smaller in the two-fluid computation than in the single-fluid MHD computation.

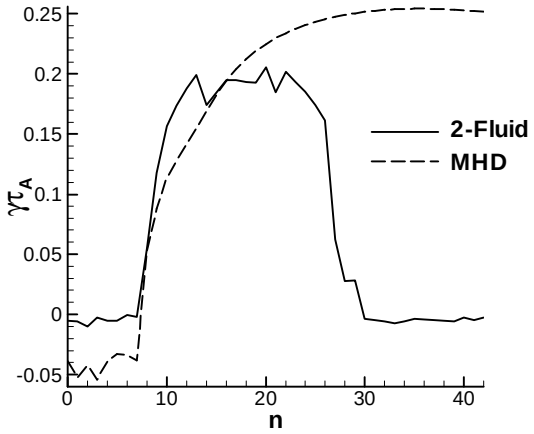

FIG 5. Comparison of two-fluid and MHD linear growth-rate spectra for toroidal wavenumbers 0≤n≤42 obtained with the parameters of the nonlinear two-fluid simulation of Sect. 5.

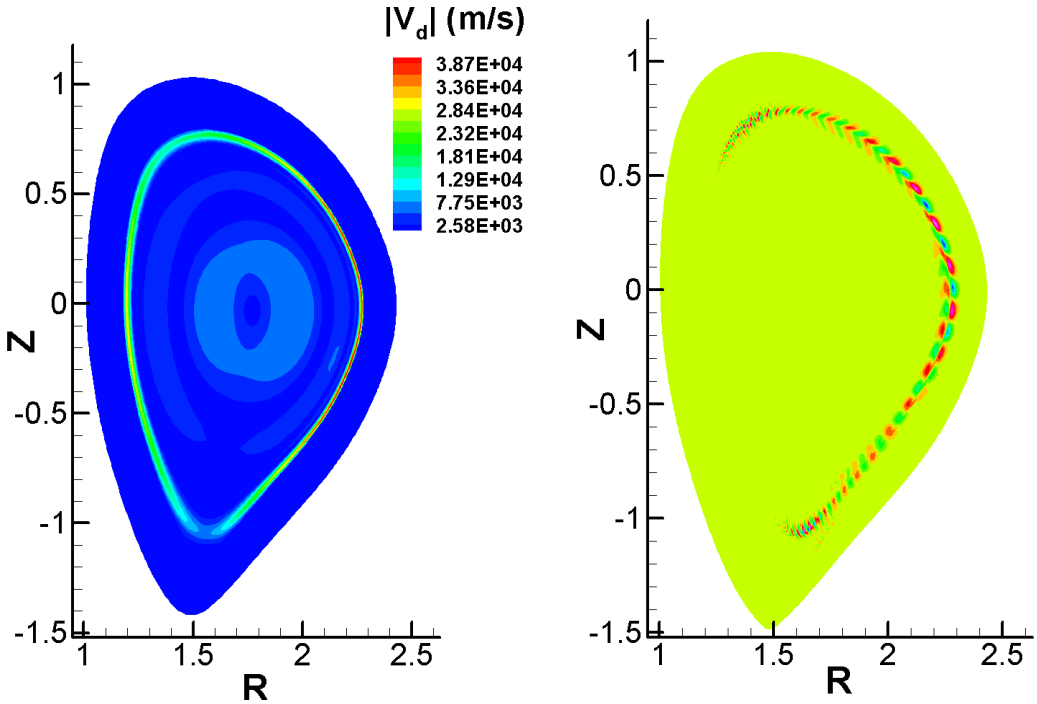

FIG 6. Poloidal component of diamagnetic drift velocity (left) and toroidal component of flow velocity for the n=21 eigenfunction computed with the two-fluid model. Compare with Fig. 4.

3. Nonlinear Results

The two-fluid computation is based on the equilibrium data for the DIII-D discharge 113317 (see Fig. 2), has dissipation coefficients of $\chi_{\|}=1.5\times10^{7}$ m^2/s, $\chi_{\perp}=1.5$ m^2/s, and $\nu=25$ m^2/s,

and uses a poloidal mesh of 20×120 biquintic finite elements. At this resolution and D=2.5 m^2/s, linear growth rates are accurate to 35% in comparison with converged results. (The particle diffusivity of 5 m^2/s is used in the nonlinear two-fluid computation.) The quantitative error from the reduced resolution does not affect the shape of the linear spectrum, however, and we expect the primary features of the nonlinear evolution to be valid at least qualitatively. Initial conditions use the results of the linear two-fluid spectrum computation shown in Fig. 5. The perturbation energies are slightly peaked toward the low end of the unstable group of modes, because they are first to emerge from the random perturbations used to initiate the linear calculations and thus have a head start in the nonlinear computation. Their amplitude at the beginning of the nonlinear computation is a somewhat arbitrary choice, as long as it does not lead to strong nonlinear effects immediately. The evolution of kinetic fluctuation energies over the first nonlinear time-steps shows two-wave coupling producing a high-n harmonic of the spectrum peak and coupling to n-values below 10 (Fig. 7), but significant growth still follows before distortions of the pedestal gradients become apparent.

In the final state of the two-fluid computation presented here, the fluctuations are growing at a decreasing rate, and density and temperature perturbations approach the pedestal values for number density and temperature. From configuration space, we observe that the perturbations do not extend over the entire outboard side of the torus, unlike the single-fluid MHD results. Instead, they are grouped into a helical band, as shown in Figs. 8 and 9. In the DIII-D 113317 equilibrium, the ELMs are resonant near q=3, and the poloidal cross-section (Fig. 8) shows three groups of perturbations: one near the separatrix, another on the outboard side above the midplane, and the third at the top of the separatrix. With respect to nonlinear coupling to low-n leading to localization, this result shares features found with the reduced-Braginskii model applied to harmonics of n=5 [4]. Although it is not filamentary, the nonlinear structure in our full-geometry computation covers only a small fraction of the toroidal angle. We note, however, that while the phases of the initial perturbations have not been prearranged, it remains to be verified that such localization is the result of phase locking during the evolution.

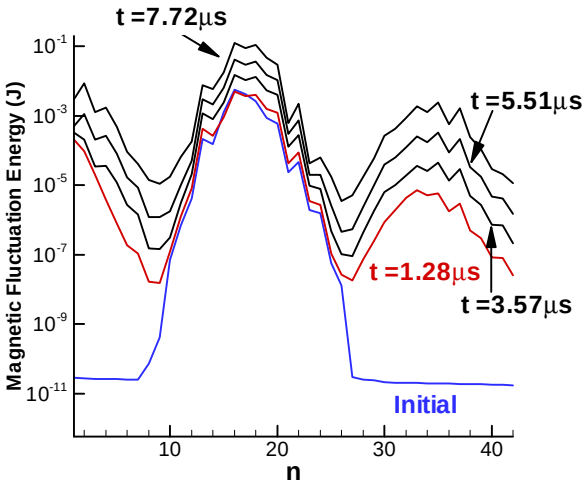

FIG 7. Evolution of the magnetic fluctuation energy from the two-fluid computation. The initial state is from the linear two-fluid spectrum calculation, and times are with respect to the start of the nonlinear simulation.

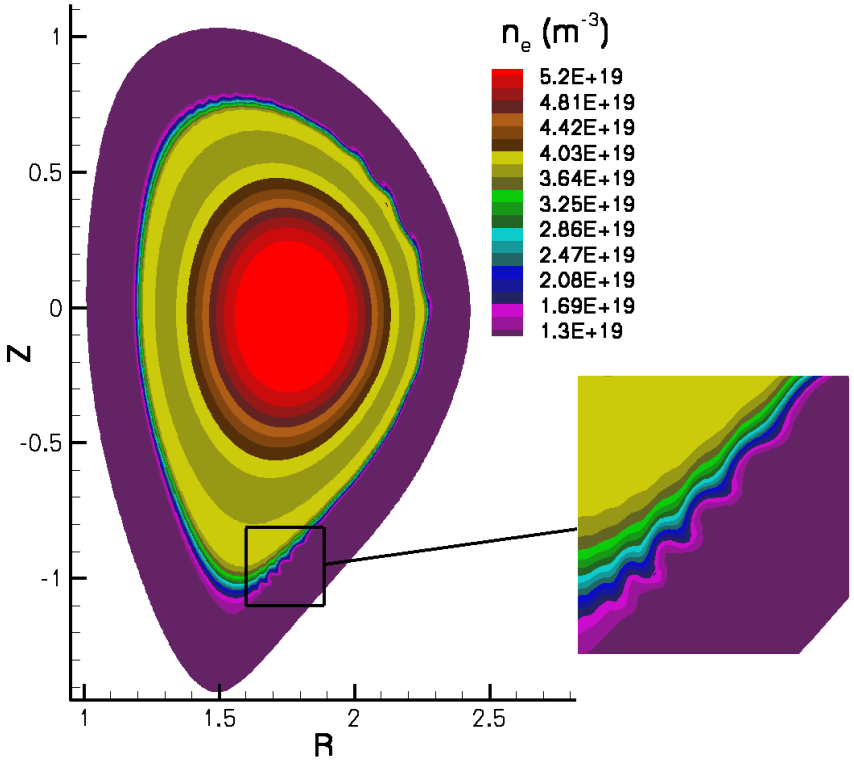

FIG 8. Number density at toroidal angle ϕ=0 at 7.92 μs into the nonlinear two-fluid computation.

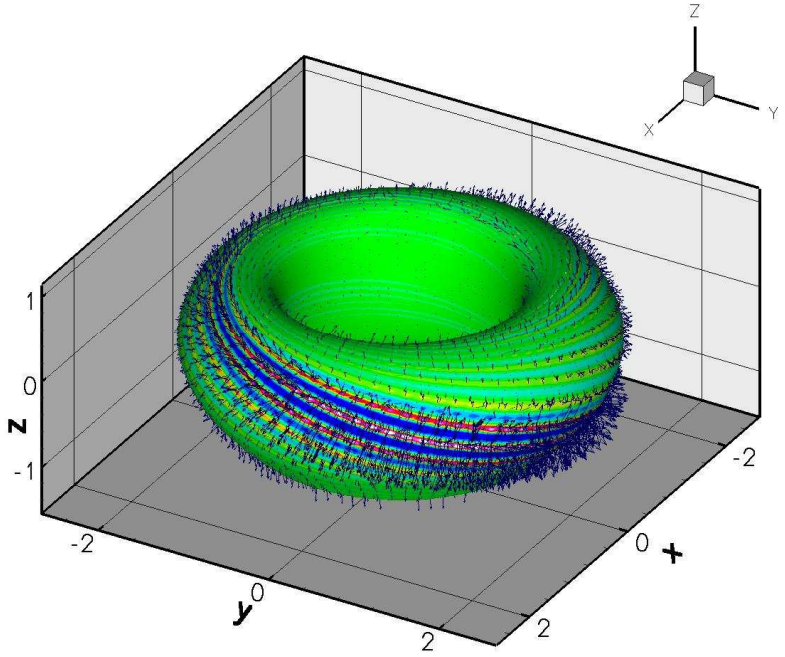

FIG 9. Temperature perturbations along the surface where n=3×10^{19} m^{-3} at 7.72 μs into the nonlinear two-fluid computation. The maximum temperature perturbation is 100 eV, 25% of the pedestal temperature. Perturbed flow velocity vectors are superposed.

4. Discussion and Conclusions

The initial linear results with the DCON, BALOO, and ELITE codes show that the peeling stability threshold for the ITER equilibrium is close to the stability threshold of a high triangularity DIII-D discharge.

To include more effects, time-dependent computations are performed with the NIMROD code. Our convergence studies find that modes with large poloidal wavenumbers can be computed accurately when high-order polynomials are used for basis functions. The converged results for linear resistive MHD show qualitative differences from the linear ideal-MHD results. Preliminary evidence suggests that resistive ballooning occurs in the NIMROD computations, but more work is needed to clarify this issue. Studies with the ELITE code [2, 3] use a simple analytic dispersion relation [12] that approximately takes into account with analytical calculations that consider the narrow diamagnetic flow profile of H-mode plasmas [13]. However, NIMROD is able to take this into account fundamentally.

The nonlinear two-fluid simulation presented here is at the forefront of the capabilities of nonlinear magnetofluid codes. It required significant computational resources in addition to recent algorithm development. Although in many ways preliminary, the results show that the numerical tools for studying the nonlinear behavior of peeling-ballooning modes with a complete two-fluid model are available. Already, we have found that coupling among the unstable band of modes at intermediate n-values generates harmonics in the linearly stable range of wavenumbers (n>30 for the case considered). The nonlinear coupling also produces an n=1 distortion. The unstable modes are resonant at or near the q=3 surface, so the n=1 distortion induces an m=3 pattern in poloidal angle. This collects fine-scale spatial oscillations into a localized helical structure as the perturbation amplitude approaches the level of the density and temperature pedestal of the equilibrium.

Acknowledgments

The authors wish to thank Chris Hegna and Jim Callen of the University of Wisconsin for many helpful discussions on physics relevant to ELMs. The authors also wish to thank Tom Osborne of General Atomics for assistance with the equilibrium information. This research used resources of the National Energy Research Scientific Computing Center, which is supported by the Office of Science of the U.S. Department of Energy under Contract No. DE-AC02-05CH11231.

References

[1] FEDERICI, G., *et.al.*, Plasma Phys. Cont. Fusion **45**, 1523 (2003).
[2] SNYDER, P. B. *et al.*, Physics of Plasmas **9**, 2037 (2002).
[3] WILSON, H. R. *et.al.* Physics of Plasmas **9**, 1277 (2002).
[4] SNYDER, P.B. *et.al.* Physics of Plasmas **12**, 056115 (2005).
[5] PANKIN, A.Y., *et.al.*, Nucl. Fusion **46**, 403 (2006).
[6] SOVINEC, C.R., *et.al.*, J. Comp. Phys., **195**, 355 (2004).
[7] SCHNACK, D.D. *et al.*, Phys. Plasmas **13**, 058103 (2006).
[8] WESSON, J.A., Tokamaks (Clarendon Press: Oxford, 1997).
[9] GLASSER, A.H., and CHANCE, M.S., Bull. Am. Phys. Soc. **42**, 1848 (1997).
[10] MILLER, R.L., and VANDAM, J.W., Nucl. Fusion **27**, 2101 (1987).
[11] PANKIN, A.Y., *et.al.*, Plasma Phys. Cont. Fusion **47**, 483 (2005).
[12] ROBERTS, K. V. and TAYLOR, J. B., Physical Review Letters **8**, 197 (1962).
[13] HASTIE, R. J., CATTO, P. J., and RAMOS, J. J., Physics of Plasmas **7**, 4561 (2000).